FliPASED
WWW.FLIPASED.EU

D2.4 Validation of the Integrated Design Toolchain for Collaborative Design

Thiemo Kier, Yasser Meddaikar, Matthias Wuestenhagen (DLR), Charles Poussot-Vassal (ONERA), Sebastian Koeberle, Julius Bartasevicius, Fanglin Yu (TUM), Balint Vanek, Daniel Balogh, Tamas Luspay, Bela Takarics (SZTAKI)

GA number: 815058
Project acronym: FLIPASED
Project title: FLIGHT PHASE ADAPTIVE AEROSERVO-ELASTIC AIRCRAFT DESIGN METHODS
Funding Scheme: H2020 **ID:** MG-3-1-2018
Latest version of Annex I: 1.2 released on 13/12/2022
Start date of project: 01/09/2019 **Duration:** 46 Months

Lead Beneficiary for this deliverable:	SZTAKI
Last modified: 29/06/2023	**Status:** Delivered
Due date: 28/02/2023	

Project co-ordinator name and organisation: Bálint Vanek, SZTAKI
Tel. and email: **+36 1 279 6113** vanek@sztaki.hu
Project website: www.flipased.eu

Dissemination Level		
PU	Public	X
CO	Confidential, only for members of the consortium (including the Commission Services)	

“This document is part of a project that has received funding from the European Union’s Horizon 2020 research and innovation programme under grant agreement No 815058.”

Glossary

ASE	Aeroservoelastic
BDF	Bulk Data File
CAD	Computer-aided Design
CAE	Computer-aided Engineering
CFD	Computational Fluid Dynamics
CPACS	Common Parametric Aircraft Configuration Schema
DLM	Doublet Lattice Method
FE	Finite Element
FEM	Finite Element Method
FEMU	Finite Element Model Updating
GLA	Gust Load Alleviation
GVT	Ground Vibration Test
HIL	Hardware-in-the-loop
LTI	Linear Time Invariant
MAC	Modal Assurance Criterion
MDO	Multidisciplinary Design Optimization
MLA	Manoeuvre Load Alleviation
RCE	Remote Component Environment
UAV	Unmanned Aerial Vehicle
XML	Extensible Markup Language

Table of contents

List of Figures

1 Executive Summary

The objective of the deliverable is to conduct a comprehensive comparison of results and findings obtained from various sources. The primary purpose of this specific assessment is to instill confidence in the developed tools and methods for the collaborative design toolchain.

The data acquired from flight tests will serve as a reference point for validating models related to structural dynamics, aerodynamics and controls. To facilitate this validation process, analysis tools will be designed for test and simulation results. For the structural dynamics tools will be available in Nastran which can be tuned based on available ground testing data. For the aerodynamics the output of different tools will be compared with flight test data gathered for the demonstrator aircraft. Furthermore, the results of the different methods available for flutter analysis will be cross-compared in order to gain confidence in the aeroelastic modeling at different stages of the collaborative design toolchain.

The proposed approach of model validation allows a thoroughly examination of the tools and methods, which are chosen for the collaborative design toolchain.

2 Overall Architecture and Tools to connect MDO and Testing

This section provides an overview of the Multidisciplinary Design Optimization (MDO) toolchain and the tools utilized within it. Each block of the toolchain is briefly introduced, along with an explanation of the interconnection between the MDO, Hardware-in-the-Loop (HIL) test, and flight test toolchains.

2.1 Overall Architecture and Tools of MDO Toolchain

The central component in this scenario is the MDO toolchain, which encompasses its own optimization process and returns to the Common Parametric Aircraft Configuration Schema (CPACS) generation block after each iteration. The primary objective of the MDO toolchain is to demonstrate the enhancements achieved through optimization, encompassing aircraft geometry, sizing, modeling, and control design concurrently, in comparison to the reference aircraft. The overall architecture of the MDO toolchain is illustrated in Figure 1.

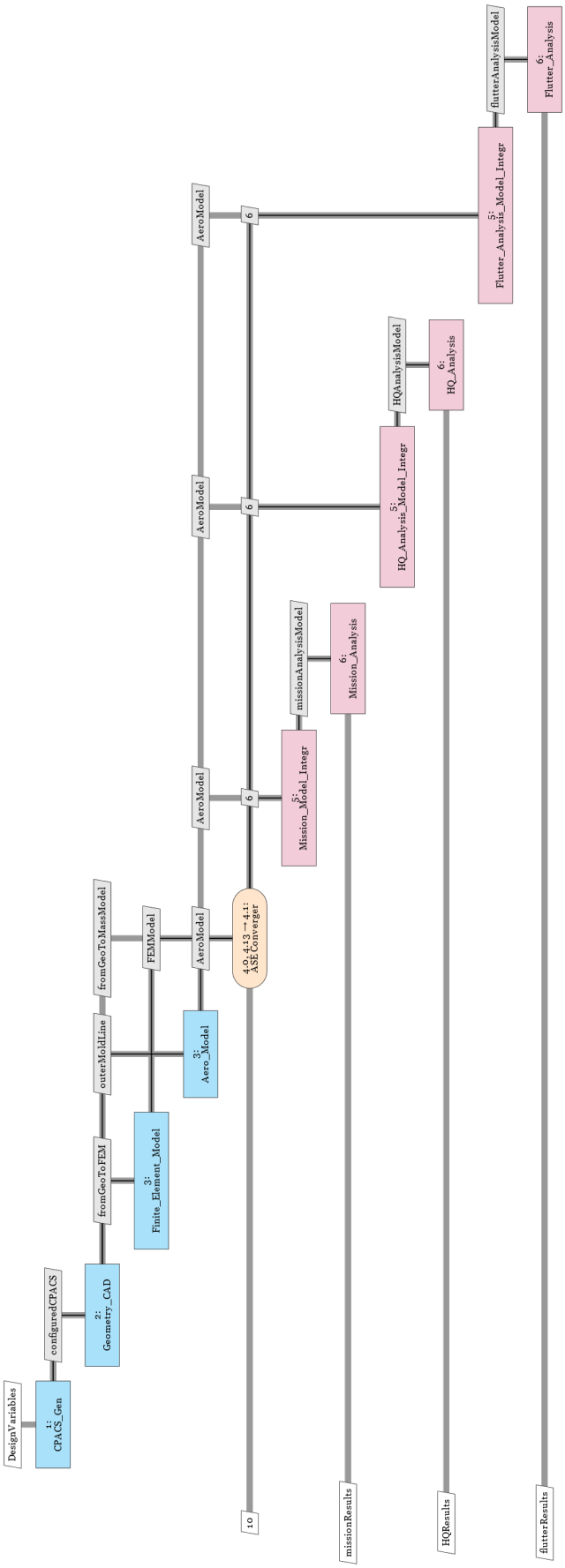

Figure 1: MDO Toolchain for demonstrator T-FLEX

The subsequent sections will provide a concise overview of the function blocks within the MDO toolchain and the standard tools employed. For more detailed information, please refer to the previous deliverables from the project, specifically D1.2, D1.4, D2.2, and D4.1.

2.1.1 CPACS

CPACS, the data model introduced and developed at the DLR since 2005, utilizes an extensible markup language (XML) implementation. The structure of CPACS follows a top-down approach, leveraging the hierarchical nature of XML's data representation. This approach involves decomposing a generic concept (such as an aircraft) into more detailed descriptions of its components. This methodology aligns with the conceptual and preliminary design stages of an aircraft, where the level of detail initially starts low and progressively increases throughout the design process. The hierarchical structure of CPACS also facilitates ease of use as an exchange format within collaborative design environments. It allows various stakeholders to effortlessly append their results due to the simplicity and compatibility of the format. As such, CPACS serves as the designated data model within this toolchain.

2.1.2 RCE

The Remote Component Environment (RCE) [2], developed by the DLR, is an open-source software environment designed for creating and running workflows that involve distributed simulation tools. RCE achieves this by integrating these tools into a peer-to-peer network. Within this toolchain, RCE serves as the integration platform, facilitating the seamless collaboration and interaction of various simulation tools.

2.1.3 CPACS generation block

The CPACS generation block, positioned as the initial block in the MDO toolchain, serves the purpose of generating the CPACS dataset utilizing the tixi library. The CPACS dataset encompasses crucial information pertaining to the geometry and structural characteristics of the demonstrator. Furthermore, it also serves as a repository documenting the information relevant to the parameter study conducted.

2.1.4 Geometry block

The Geometry block is designed to facilitate the updating of the Catia model based on the incoming CPACS file from the upstream CPACS generation block. Its primary objective is to examine the modifications within the geometry and make corresponding updates to the Catia model. By comparing the incoming CPACS file with the existing model, the Geometry block ensures that any changes in the geometry are accurately reflected in the Catia model. This synchronization process enables the model to stay up to date with the most recent design specifications and ensures consistency between the CPACS dataset and the Catia model.

2.1.5 FE model block

The finite element (FE) model block serves two primary functions in the workflow. First, it is responsible for meshing the geometry model obtained from Catia. This involves dividing the geometric representation into discrete elements or nodes to create a FE mesh. The meshing process is crucial for accurate structural analysis and simulation.

In addition to meshing, the FE model block also assigns structural properties to the meshed elements. This step involves defining material properties, such as elasticity, density, and other relevant parameters, to ensure accurate representation of the physical behavior of the structure during analysis.

Furthermore, within the FE model block, a Splining model is generated. The Splining model is a valuable component that couples the structural and aerodynamic models. It allows for the integration of aerodynamic forces and loads into the structural analysis, enabling a comprehensive understanding of the interactions between the structure and the surrounding airflow.

Overall, the FE model block plays a crucial role in preparing the geometry for analysis by meshing it, assigning appropriate structural properties, and generating a Splining model to capture the coupled effects of aerodynamics and structural behavior.

2.1.6 Aero model block

The aero model block operates by taking the geometry definition from the CPACS file as input. Its primary function is to generate the Doublet Lattice Method (DLM) aerodynamic model based on this input geometry. Once the DLM aerodynamic model is generated, the aero model block exports it to a Nastran Bulk Data File (BDF) format. By exporting the DLM aerodynamic model to a Nastran BDF file, it becomes compatible with the Nastran software for further analysis and integration with the structural model.

In summary, the aero model block takes the geometry definition from the CPACS file, generates the DLM aerodynamic model, and then exports it to a Nastran BDF file format. This allows for seamless integration of the aerodynamic model with the structural analysis workflow using Nastran.

2.1.7 Aeroelastic Model Generation and Simulation

This block utilizes aerodynamic, structural, and spline grid information, along with mass and stiffness matrices, to generate a Simulink model. The generated Simulink model is then employed for control synthesis design purposes.

2.1.8 Baseline and Flutter Suppression Control Design Blocks

The block the aerodynamics and structural dynamics model data delivered from the previous block by DLR-SR. Based on this data the block first generates two models: a quasi rigid body model with the 12 rigid body states for the baseline control design and one low order aeroelastic model for the flutter suppression control design. The baseline controller is designed next based on the 12 state model. Since the rigid body model can have unstable rigid body modes, which the baseline controller stabilises, it is crucial to use the inner loops of the baseline controller for the flutter suppression design. Therefore, the inner loops of the baseline controller is connected to the low order flexible model and then the flutter controller is synthesized for this model. Finally, the analysis block receives the full baseline controller, the flutter controller and the flexible model and the robustness margins of the closed loops are assessed. Based on this, the open loop flutter speed and the achieved closed loop robust flutter speeds can be evaluated. Below is a short evaluation of the results of a parameter study. The flutter mass and the sweep angles were varied as presented in Table 1.

Table 1: Demonstrator RCE results

Flutter mass [kg]	Sweep angle [deg]	Open loop flutter speed [m/s]	Closed loop robust flutter speed [m/s]	Gain in flutter speed [%]
0.24	20	56	65	16.07
0	20	≥ 70	≥ 70	–
0.12	20	66	≥ 70	–
0.36	20	50	59	18
0.24	0	53	63	18.87
0.24	10	53	62	16.98
0.24	15	53	63	18.87
0.24	25	58	62	6.9
0.24	30	61	66	8.2

It can be seen that the modeling for the baseline and flutter control design, both control design tools and the analysis run successfully in an automated fashion for all parameter variations.

2.2 Connection between MDO Toolchain and Testing

The HIL test and flight test blocks play crucial roles in validating the developed methodologies, as depicted in Figure 2.

The HIL tests focus on evaluating the practical implementation aspects of the controllers, serving as a final step before conducting flight tests.

In the case of the MDO toolchain, flight tests serve two primary objectives. Firstly, they validate the maturity of the control design technology, particularly for the manoeuvre load alleviation (MLA), gust load alleviation (GLA), and flutter suppression controllers, which have not undergone flight testing using the model-based design methodology within FLiPASED. Secondly, flight tests provide an opportunity for fine-tuning the controllers manually to achieve optimal performance and gain valuable insights for both the designers (making the models and the controllers) and the broader aviation community. In this context, the automatic execution of the synthesis algorithms is not a critical criterion, as the focus lies on optimizing controller performance based on the updated aircraft model derived from flight test data.

At the conclusion of the cycle, the lessons learned from the HIL tests and flight tests are fed back into the MDO toolchain through engineering considerations. If the HIL tests identify any implementation challenges with specific controllers, the corresponding control design algorithms need to be updated. Similarly, if the flight tests reveal performance or robustness issues with a controller, the algorithms must be adjusted accordingly.

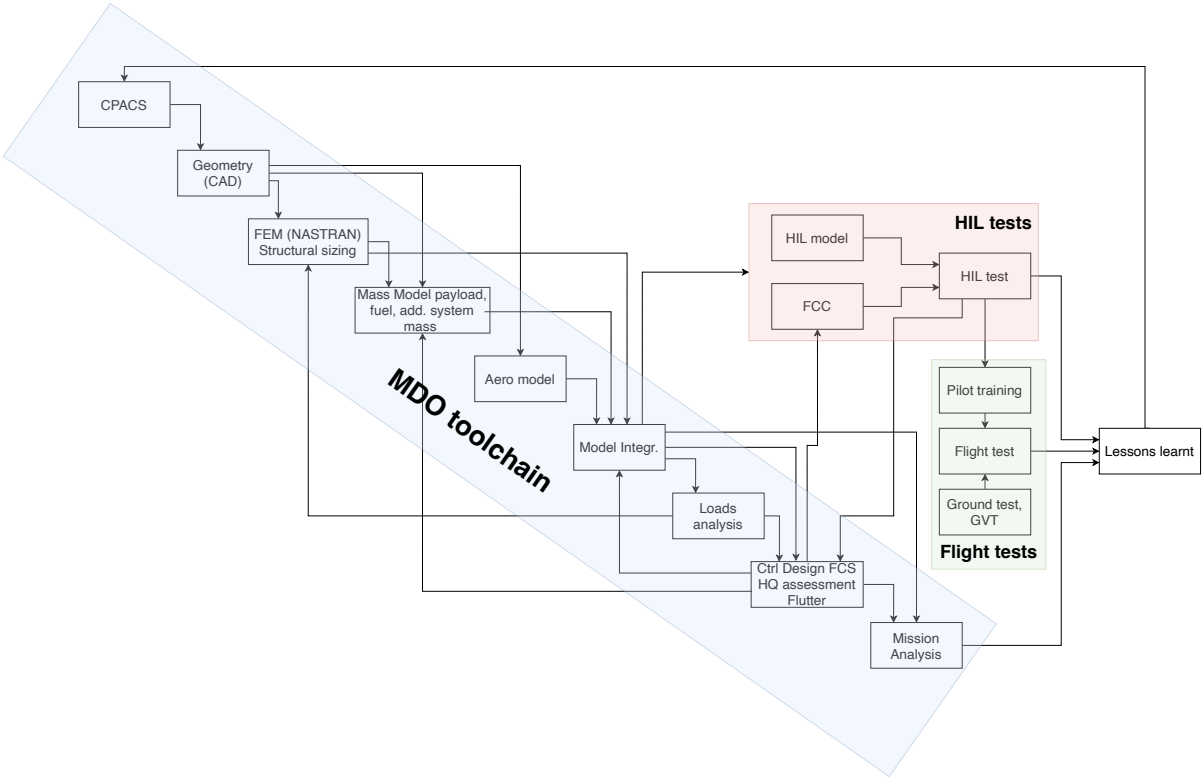

Figure 2: Toolchains developed in FLiPASED

In the following sections a more detailed explanation regarding toolchain validation is provided.

3 Structural Dynamics Model Validation

The tasks related to structural dynamics of the aircraft models are led by DLR-AE, but contributions are made by ONERA, TUM, SZTAKI and DLR-SR as well.

The main steps regarding the task are:

- structural model development and ground vibration test (GVT) based update
- Model comparison and fine tuning for RCE toolchain based and GVT based model matching
- Operational modal analysis based model update during flight tests and its connection how this feeds back to NASTRAN models
- Description of used tools and how they can we standardized

In this chapter, a summary of the structural dynamics model and the model-updating activities pertaining to its update are described.

3.1 NASTRAN structural dynamic model

The structural dynamic models of the T-Flex aircraft are developed using a modelling toolchain established during FLEXOP and FLiPASED. In total, three pairs of wings are designed, manufactured and tested on the unmanned aerial vehicle (UAV) test-bench:

(i) wings -0 - a pair of wings optimized using balanced-symmetric type of laminates serving as the reference wing

(ii) wings -1 - a pair of flutter wings designed to trigger flutter within the test-regime, whose flight envelope will then be extended using active flutter control

(iii) wings -2 - a pair of wings optimized using unbalanced composite laminates, to demonstrate passive load alleviation through aeroelastic tailoring

The structural FE models for the wing pairs -0 and -2 are generated using an in-house model generator ModGen at DLR-AE [3], while those of the -1 wing are obtained from a CAD-FEM toolset at TUM. The wing models are integrated to the fuselage and empennage models generated during FLEXOP at DLR-AE. The fuselage and empennage models are also generated using ModGen [3].

3.2 Model-updating of the -0 wings

A ground-test campaign [5] involving structural tests and GVTs has been performed on the T-Flex aircraft. An update of the FE model of the -0 wing has been performed based on experimental data and is presented in this section.

Three different methodologies for finite element model updating (FEMU) using Nastran were developed: i) a simultaneous approach, ii) a static and dynamic separated approach, and iii) an approach with two static steps and then dynamic FEMU. The overall implementation of FEMU in Nastran is shown in Figure 3.

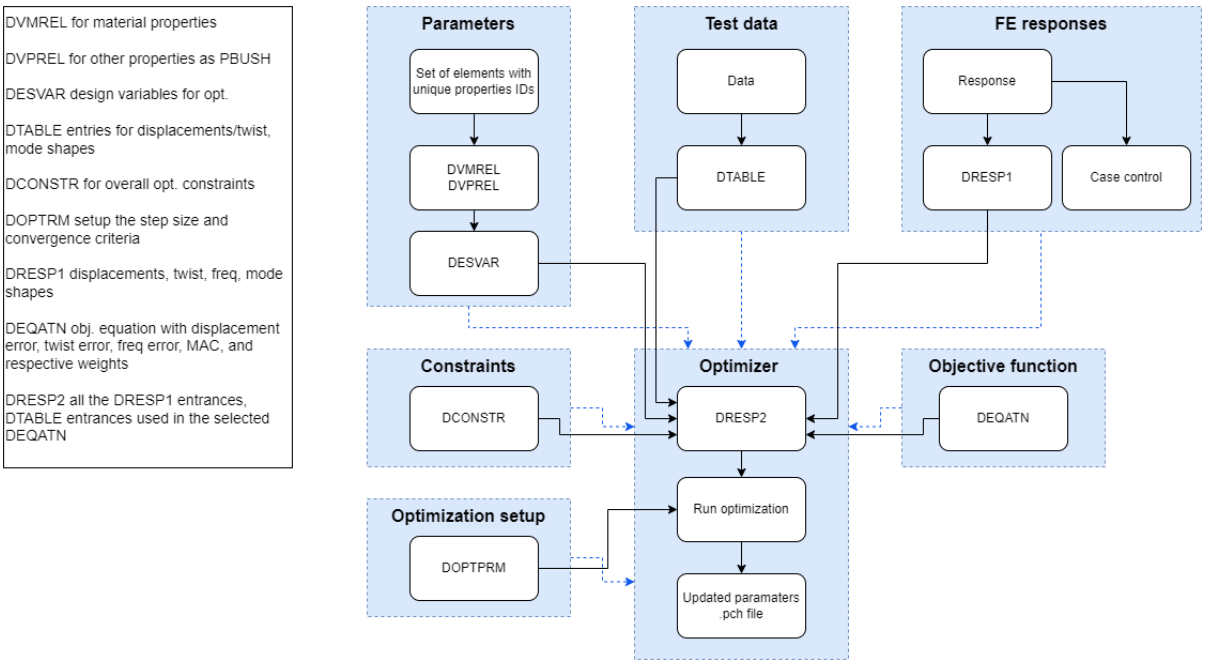

Figure 3: Schematic diagram of FEMU implementation in Nastran

The simultaneous approach used the GVT and static data to formulate the FEMU optimization problem in one step. This method could not generate results due to limitations in the mode tracking capability inside Nastran. Nastran was not able to track the structural eigenmodes from one iteration to another during the optimization process, even though the step size of the parameter change per iteration was significantly reduced.

The second approach divides FEMU into a static FEMU and then a dynamic FEMU. It has the advantage that the dynamic update does not change the static behavior of the structure and that the Nastran mode tracking capability works if, in the dynamic FEMU, the step of parameter change between iterations is sufficiently small.

A third approach was considered to take into account the uncertainty in the modelling of the clamp attachment between the wings. In the first phase of the three steps the stiffness of the clamps of the wing is updated using static test data. This followed by the two steps similar to the second approach.

Additionally, FEMU was also tested using FEMTools. FEMTools is an independent solver and computer-aided engineering (CAE) software for the analysis of structures [1]. The model updating was divided in static and dynamic update, the static update included the static test results, while the dynamic update included GVT results.

3.2.1 Static data comparison

The updated models were compared to test points that were not used for the udpdate, namely 2.5g and 5g equivalent loads that were introduced onto the wings.

Various FE models were compared, but only few presented significant differences in the results. For example, the differences between a model that scaled the mechanical properties E_1, E_2, G_{12} of the composite material together and another that independently scaled these properties, led to results with no significant differences. Therefore, the model that scaled the mechanical properties together was chosen because this scaling has better physical meaning as it changes the composite A components from

the ABD matrix defined by composite laminate theory proportionally. The FE models that presented substantial differences were:

- Non-updated FE model
- Updated model using the static and dynamic approach (Updated all at once A matrix)
- Updated model using the two static steps and then dynamic FEMU approach (Updated 2 phases A matrix)
- Updated FEMTools using Nastran as solver

The spanwise deflection and twist angle for the 2.5G load factor are shown in Figure 4 and Figure 5 respectively. It can be observed that the FEMTools updated model is the closest to the non-updated model, and both tend to be stiffer than the experimental results, with the FEMTools updated model being slightly closer to the experimental results. In terms of deflection, the updated models using Nastran are very close together and more flexible than the experimental data. On the other hand, concerning twist angle, they tend to match the experimental data, with the two step static approach being slightly stiffer.

The spanwise deflection and twist angle for the 5G load factor are shown in Figure 6 and Figure 7 respectively. In terms of deflection, the best match with the experimental data was obtained by the FE models updated using Nastran, while the non-updated model and the FEMTools model seem to be stiffer than the experimental results. Concerning twist, all the FE models tend to be stiffer than the experiment, with the non-updated being the farthest from the experimental results, and the updated model with one static step being the closest to the test results.

Overall, it can be seen that the best performance was obtained by the FE models updated using Nastran, with the FE model that used a two step static approach having more engineering insight because of the constraints applied on the updated parameters.

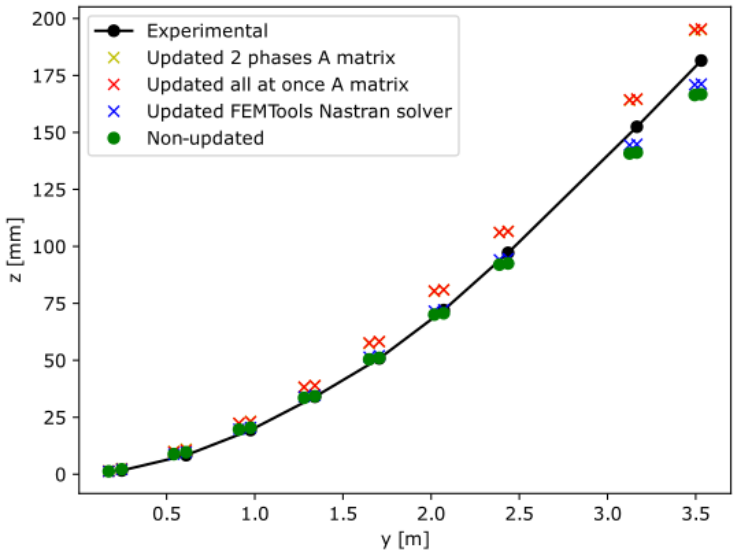

Figure 4: Spanwise deflection (z displacements) of the wing for a 2.5G load factor

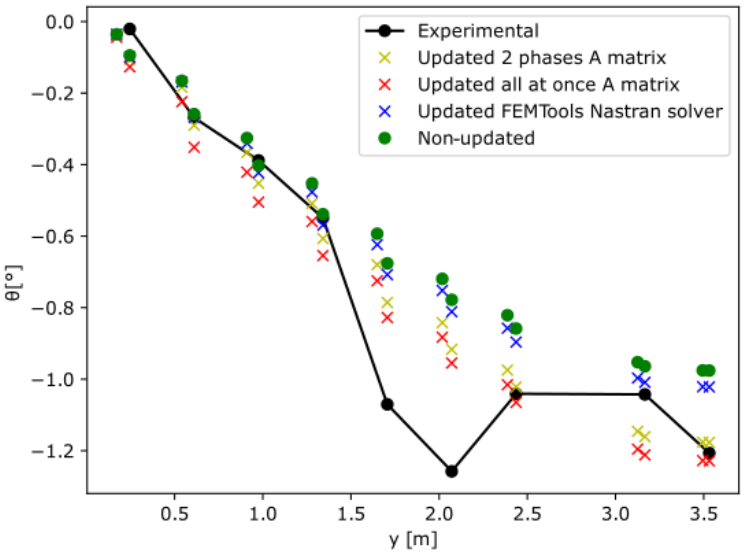

Figure 5: Spanwise twist angle θ of the wing for a 2.5G load factor

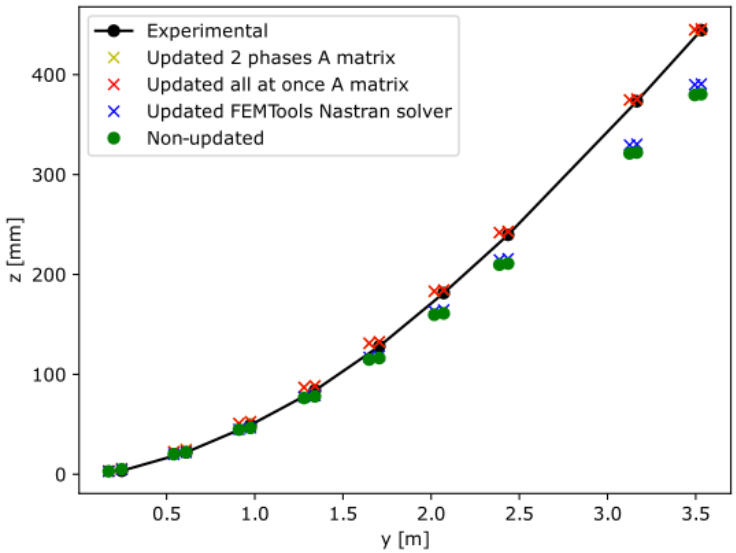

Figure 6: Spanwise deflection (z displacements) of the wing for a 5G load factor

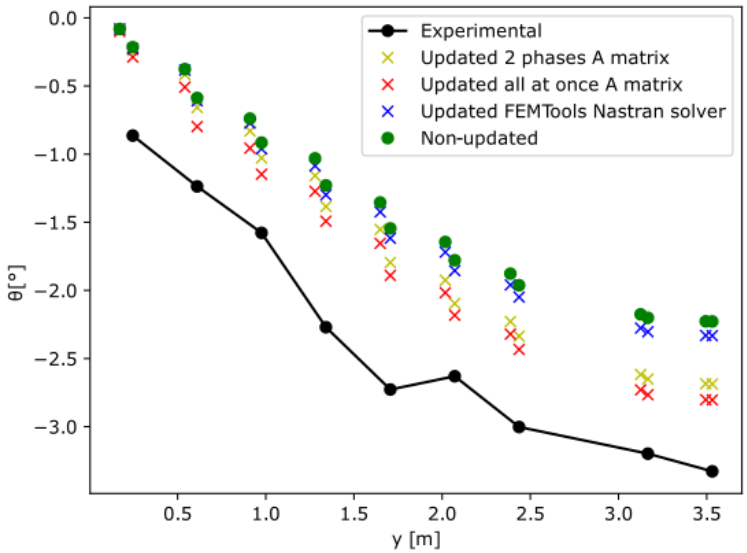

Figure 7: Spanwise twist angle θ of the wing for a 5G load factor

3.2.2 Dynamic data comparison

The first 5 non-rigid experimental mode shapes, obtained from the GVT data, were used for the dynamic behavior comparison between the FE models and the experimental data. The frequency results are presented in Table 2, and the modal assurance criterion (MAC) between the FE model and the experimental mode shapes is presented in Table 3.

From Table 2 it can be seen that the updated FE models have closer frequencies to the experimental data than the non-updated FE model. The closest frequencies were obtained by the FEMU performed in Nastran.

Concerning the mode shapes, from Table 3 it can be seen the MAC of the mode shapes did not change significantly between the updated and non-updated FE model.

Experimental		**Non-updated**		**Nastran**		**FEMTools**	
Mode	**Freq [Hz]**	**Freq [Hz]**	**Error**	**Freq [Hz]**	**Error**	**Freq [Hz]**	**Error**
6	3.37	3.56	5.6%	3.37	0.0%	3.16	6.2%
7	8.27	9.17	10.8%	8.42	1.7%	7.85	5.1%
9	12.12	12.93	6.7%	12.10	0.1%	11.47	5.4%
11	19.26	19.86	3.1%	19.18	0.4%	18.34	4.8%
12	23.00	26.43	14.9%	26.11	13.5%	20.60	10.5%

Table 2: Frequency comparison for the first 5 non-rigid experimental modes

Mode	Non-updated	Nastran	FEMTools
6	0.96	0.96	0.96
7	0.95	0.95	0.95
9	0.95	0.95	0.95
11	0.44	0.44	0.44
12	0.93	0.92	0.89

Table 3: MAC between the different FE models and the experimental data for the first 5 non-rigid experimental modes

3.3 Comparison of -1 aircraft structural dynamic model with static test

The FLEXOP project conducted a comprehensive static test of the -1 wing simultaneously with the -0 and -2 wings. The primary objective was to verify the stiffness properties of the manufactured wing and validate the accuracy of the FE model developed during the design stage.

Figure 8 illustrates the wing tip deflection at different load cases, showcasing the linear relationship between the applied load and deflection. However, it is important to note that due to measurement errors, a zero drift was observed when the load was increased from zero and then decreased back to zero.

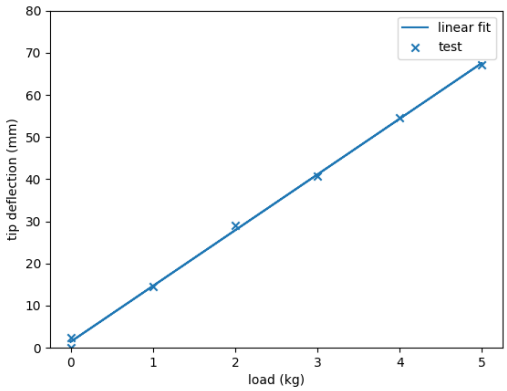

Figure 8: Displacement vs load at tip of the wing from static tests (-1 wing)

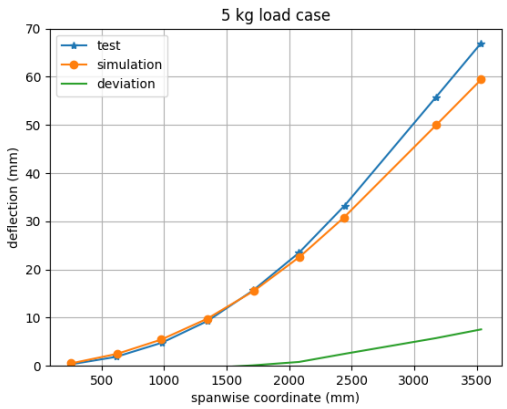

Figure 9: Span-wise displacement of wing under tip load (-1 wing)

To replicate the static test, the FE model was refined and adjusted. A comparison between the simulation and the actual test was conducted, focusing on the span-wise displacement of the wing under a 5 kg tip load (Figure 9). The results revealed that the manufactured wing exhibited greater flexibility than initially modeled, showing a similar trend to the -0 and -2 wings. The deviation between the simulation and test results was approximately 12%, not accounting for the zero drift observed during the test.

Furthermore, the torsional load cases were also investigated. Figure 10 demonstrates the linearity of the model under various torque loads. A comparison of the span-wise torsion of the wing under a 2 kg torque load (Figure 11) revealed minimal differences of only 0.1 degrees. Taking into account the inherent measurement errors, the simulation and test results aligned quite well.

These static test findings provide valuable insights into the stiffness properties and structural behavior

of the -1 wing. The significant flexibility observed in the manufactured wing highlights the importance of real-world testing and serves as a basis for further design refinements. By enhancing the accuracy of the FE model and addressing the observed deviations, future optimizations can be made to improve the wing's performance and ensure its reliability during flight operations.

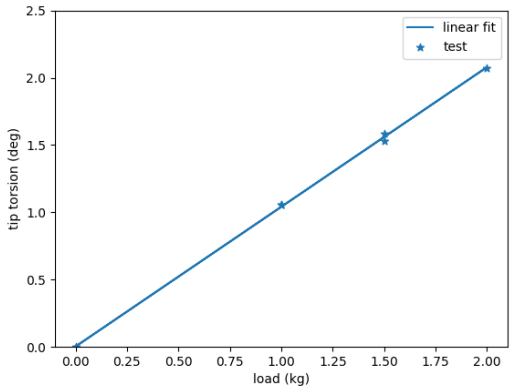

Figure 10: Torsion vs load at tip of the wing from static tests (-1 wing)

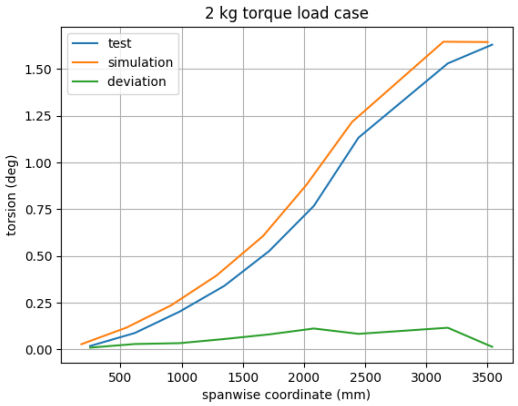

Figure 11: Span-wise torsion of wing under tip load (-1 wing)

3.4 Comparison of -1 aircraft structural dynamic model with GVTs

The generation of the -1 wing FE model was carried out at TUM using a CATIA-Hypermesh toolset. This highly detailed model encompasses both structural and non-structural components, including on-board systems, ensuring a high-fidelity representation.

Table 4 presents a comparison of the eigen frequencies between the -1 aircraft model (without updates) and the ground vibration test (GVT) results. Generally, a good agreement is observed between the FE model and the GVT outcomes. However, two significant observations arise from this comparison.

Firstly, the third flexible mode (3n_wing_bending-a) exhibits the most notable difference between the experimental results and the GVT. Given that this wing bending mode plays a critical role in the flutter mechanisms of the -1 aircraft, it becomes crucial to update the wing FE model to accurately capture the frequency of this mode.

Secondly, the second flexible mode (1n_wing_in-plane-a) is observed during the GVT but not in the FE simulations. This mode involves relative motion between the fuselage and wing, as depicted in Figure 12. This occurrence can be attributed to some degree of free-play or softness in the attachment between the fuselage and wings, which is not accounted for in the idealized attachment assumed by the FE models. To simulate this mode, an approach under consideration involves introducing soft springs at the wing-fuselage interface to ensure its presence in the simulation. Furthermore, ongoing studies are exploring the update of the FE model to address the aforementioned mode, and the use of tuning beams is planned as part of this endeavor.

In conclusion, the comparison between the -1 wing FE model and the GVT results has highlighted the need for updates to accurately capture the critical wing bending mode and address the relative motion between the fuselage and wing. These updates, along with the incorporation of tuning beams, will contribute to improving the fidelity of the FE model and enhance its ability to simulate the aircraft's behavior more accurately.

Mode	GVT (hz)	FE (hz)	Δf (%)
2n_wing_bending-s	2.94	2.91	-1.02
1n_wing_in-plane-a	7.01	–	–
3n_wing_bending-a	7.57	8.15	7.66
wing_torsion-s	10.27	10.50	2.24
wing_torsion-a	10.73	10.61	-1.12
4n_wing_bending-s	12.13	12.11	-0.16
2n_wing_in-plane-s	15.07	15.06	-0.07

Table 4: Comparison of eigen frequencies of the flexible modes: GVT vs FE model of the -1 aircraft (*i*n - *i* nodes in the mode, s - symmetric, a - antisymmetric)

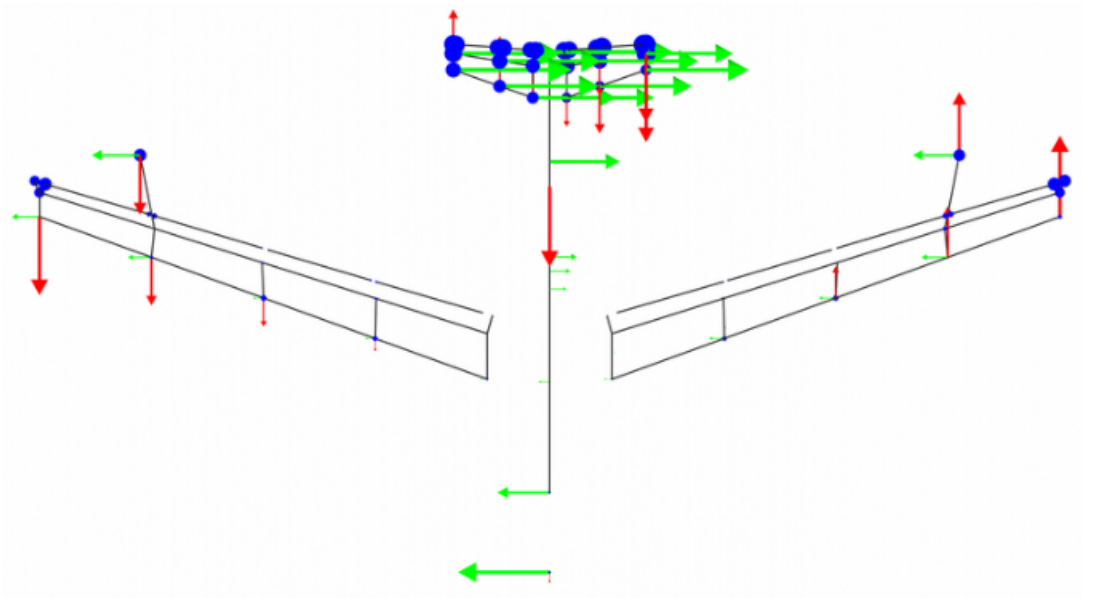

Figure 12: -1 aircraft 1n_wing_in-plane mode

3.5 Model-updating of the -1 wing

The initial model updating of the -1 wing is performed using data obtained from the static test. In this process, a knock-down factor is applied to the engineering stiffness values (E_1, E_2, G_{12}) of the wing skin and spar. The model updating procedure focuses on the 3 kg bending load case as a basis. As depicted in Figure 13, the simulation results exhibit a close resemblance to the test data. The deviation between the simulation and test results is reduced to 2mm, falling within the range of test error.

Moving forward, the torsional load case with a 2kg load is simulated using the updated model, as

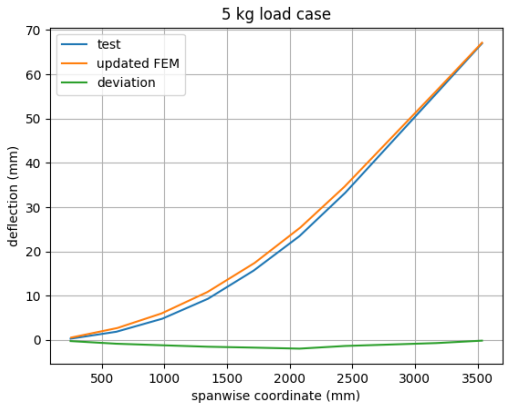

Figure 13: Span-wise displacement of wing under tip load (-1 wing)

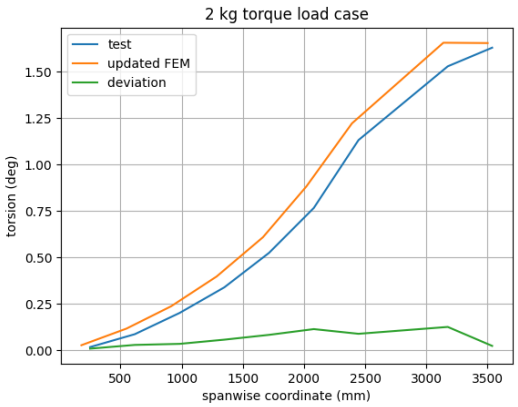

Figure 14: Span-wise torsion of wing under tip load (-1 wing)

illustrated in Figure 14. As expected, no noticeable differences are observed since the parameter updating primarily accounts for the bending load case. With the completion of the model updating process, a modal analysis is conducted using the updated model. Figure 15 presents a comparison of the eigenfrequencies among the ground vibration test (GVT) data, the original FE model, and the updated FE model.

Notably, only the 3n asymmetric wing bending mode exhibits improvement, while all other modes show a deterioration. This outcome can be attributed to the fact that the static test-based updating primarily tunes down the engineering stiffness (E_1), consequently resulting in decreased eigenfrequencies. To address this issue, the next step involves the localized implementation of tuning beams to enhance the performance of the 3n bending mode without adversely affecting the other mode shapes.

Nr	Mode	GVT	FEM	deviation %	updated FEM	deviation updated %
0	2n wing bending-s	2.94	2.91	-1.19	2.74	-6.91
1	3n wing bending-a	7.57	8.15	7.7	7.66	1.13
2	wing torsion-s	10.27	10.5	2.2	10.43	1.6
3	wing torsion-a	10.73	10.61	-1.15	10.53	-1.86
4	4n wing bending-s	12.13	12.11	-0.19	11.42	-5.83
5	2n wing inplane-s	15.07	15.06	-0.05	14.32	-4.96

Figure 15: Comparison of eigen frequencies of the flexible modes: GVT vs FE model vs updated FE model of the -1 aircraft (*i*n - *i* nodes in the mode, s - symmetric, a - antisymmetric)

3.6 Comparison of RCE aircraft model with static test and GVT

The initial model generated through the MDO toolchain was developed to simulate the static test setup. However, it was observed from Figure 16 that the RCE model exhibited significantly higher stiffness

compared to the manufactured wing. To address this discrepancy, a similar approach as the -1 wing updating process was employed, applying a knock-down factor to the engineering stiffness of the wing spar and skin. As illustrated in Figure 17, the results of the wing bending simulation with the updated RCE model show a much closer alignment with the static test results.

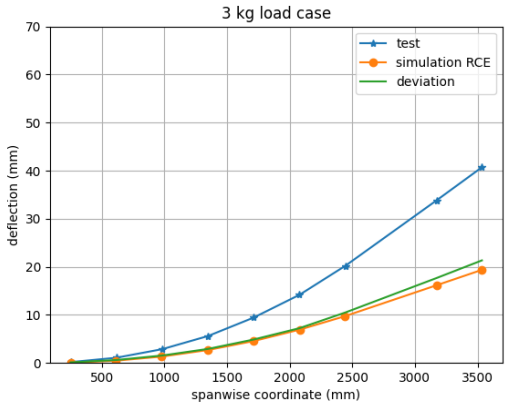

Figure 16: Span-wise bending of wing under tip load (-1 wing RCE model)

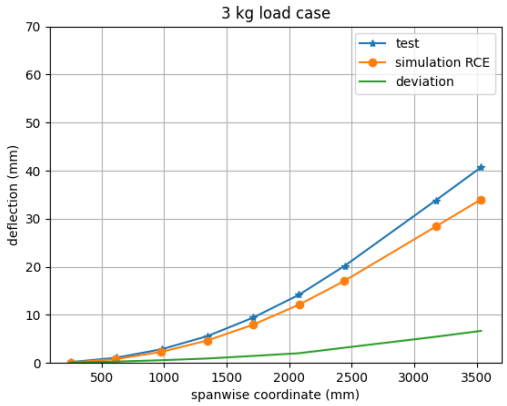

Figure 17: Span-wise bending of wing under tip load (-1 wing RCE updated model)

Additionally, a modal analysis was conducted for both the initial RCE model and the updated RCE model. The outcomes of this analysis can be observed in Figure 18. Notably, following the update, improvements were observed in all the listed modes, indicating a better alignment between the simulation and test data.

Nr	Mode	GVT	RCE FEM	deviation %	updated RCE FEM	deviation updated %
0	2n wing bending-s	2.94	3.81	29.68	2.89	-1.54
1	3n wing bending-a	7.57	10.05	32.82	7.8	2.99
2	wing torsion-s	10.27	12.25	19.3	10.65	3.74
3	wing torsion-a	10.73	12.7	18.33	10.86	1.24
4	4n wing bending-s	12.13	17.38	43.31	13.25	9.25
5	2n wing inplane-s	15.07	17.86	18.54	14.43	-4.27

Figure 18: Comparison of eigen frequencies of the flexible modes: GVT vs RCE FE model vs updated RCE FE model of the -1 aircraft (*i*n - *i* nodes in the mode, s - symmetric, a - antisymmetric)

3.7 Validation of the low order aeroservoelastic model

The last step is to validate the accuracy of the low order aeroservoelastic (ASE) model that is constructed in the modeling block of the RCE framework. This model serves as the basis for the automatic baseline and flutter suppression control design algorithms. The model is a set of linear time invariant (LTI) models that are obtained form the nonlinear model by Jacobian linearization at airspeed values

between 38 and 64 m/s. The model needs to capture the low frequency dynamics of the aircraft for the baseline control design and the flutter modes for the flutter suppression design.

The base model is the low order model of the FLEXOP aircraft that is described in [4]. The pole map trajectories (as function of the airspeed) of the base model and the RCE generated models are shown in Figure 19.

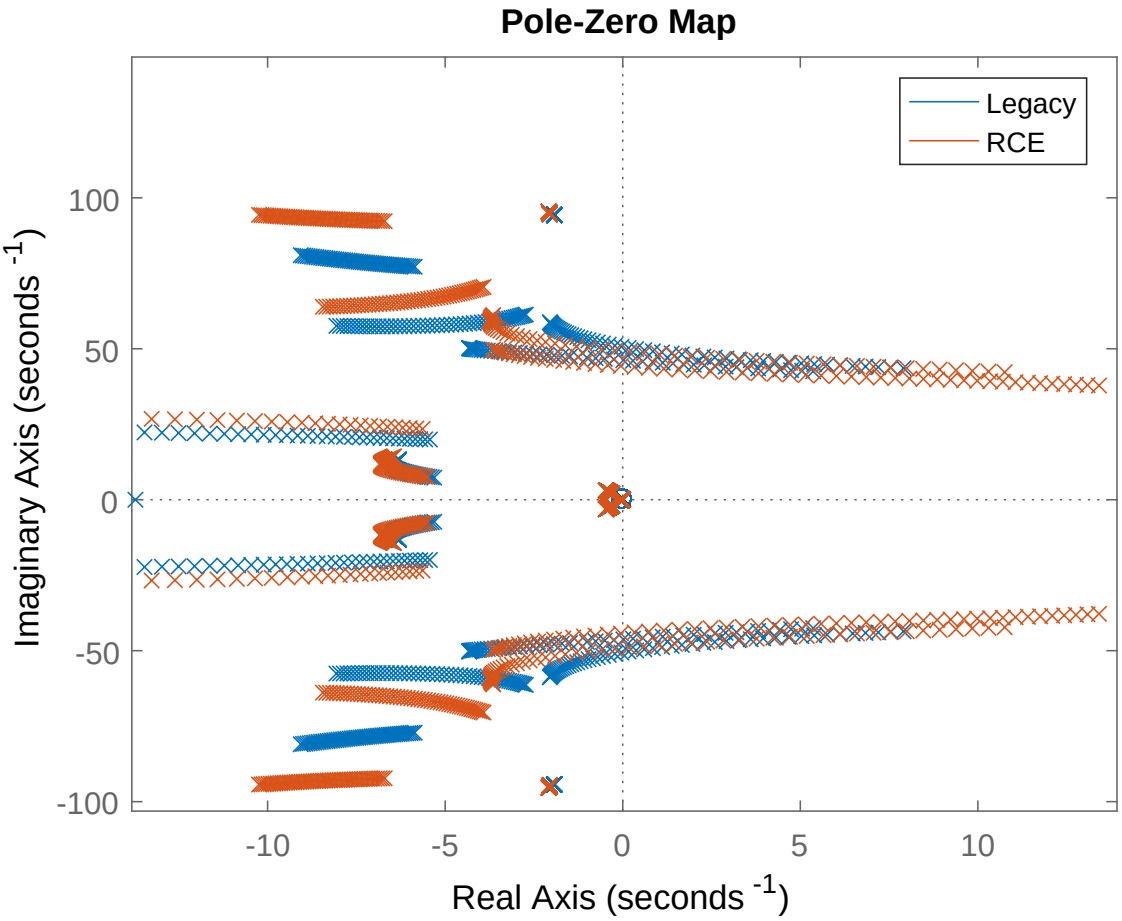

Figure 19: Comparison of pole trajectories of the ASE models: Legacy FLEXOP model vs RCE generated model of the -1 aircraft

The plots show good match between the legacy FLEXOP and the RCE generated model. The pole trajectories show similar trends and the interdependency between them is also very similar between the two modeling frameworks.

4 Flutter Analysis Validation

Within the project different partners have used different flutter analysis tools. However, they should in the end give similar results. It is therefore very straight forward to compare the results of the different methods of flutter analysis and use this as a validation of the tools and if any implementation mistakes has happened along the way.

4.1 Flutter Analysis using NASTRAN SOL145

The NASTRAN SOL145 flutter solution is used as one potential tool to evaluate the flutter stable boundary. The tool has been used for instance, to decide on safe configurations with respect to the triggerable flutter mass, as well as to compare different system configurations on the wing, for instance the design of the flutter mass trigger mechanism itself.

The flutter analysis is based on PK-solver from which the aeroelastic frequencies and damping are obtained. Shown for instance in Figure 20 is the flutter analysis for the nominal configuration with the flutter mass in its ”loaded” position and the flutter stopper mass as per the nominal design.

4.2 Flutter Analysis based on Linearised Models

The Simulink model representing the nonlinear flexible aircraft dynamics can be used in order to determine the open-loop flutter speeds and frequencies. The aircraft is trimmed and linearised for a couple of flight conditions. Especially, differences in flight speed are of interest for the demonstrator aircraft, as they have the biggest effect on the aeroelastic modes. The set of linearised state-space models is then analysed with respect to their eigenvalues. It is then possible to see the gradual change in the eigenvalues and therefore the frequency and damping for varying flight conditions as exemplary shown in Figure 21. As soon as a pole crosses the imaginary axis and migrates to the right half plane, unstable flutter becomes an issue. Based on the trimmed airspeed of the linearised systems it can then be determined what the flutter speed is. This leads then to Figure 22, which shows the damping and flutter frequency for symmetric and asymmetric flutter over the flight speed. As soon as the damping crosses the zero line the corresponding aeroelastic mode becomes unstable.

4.3 Flutter Analysis Method based on low order control oriented models

The current section describes the flutter analysis of the linearized reduced order control oriented models. These are the models that are used for the flutter suppression control design in the MDO toolchain. The overall approach is very similar to the one described in the previous subsection. The main difference is that the nonlinear Simulink model of the aircraft is constructed from reduced subsystems. In the next step the nonlinear model is trimmed and linearized over an airspeed grid between 40 and 70 m/s. Finally, the eigenvalues of the linearized models are evaluated. The flutter speed is the airspeed at which the first flutter mode becomes unstable. The results are, as expected, very similar to the results presented in the previous section. However, the flutter speed is overestimated by approximately 1 m/s. The reason for this overestimation lies in the neglected dynamics resulting from the low order modeling.

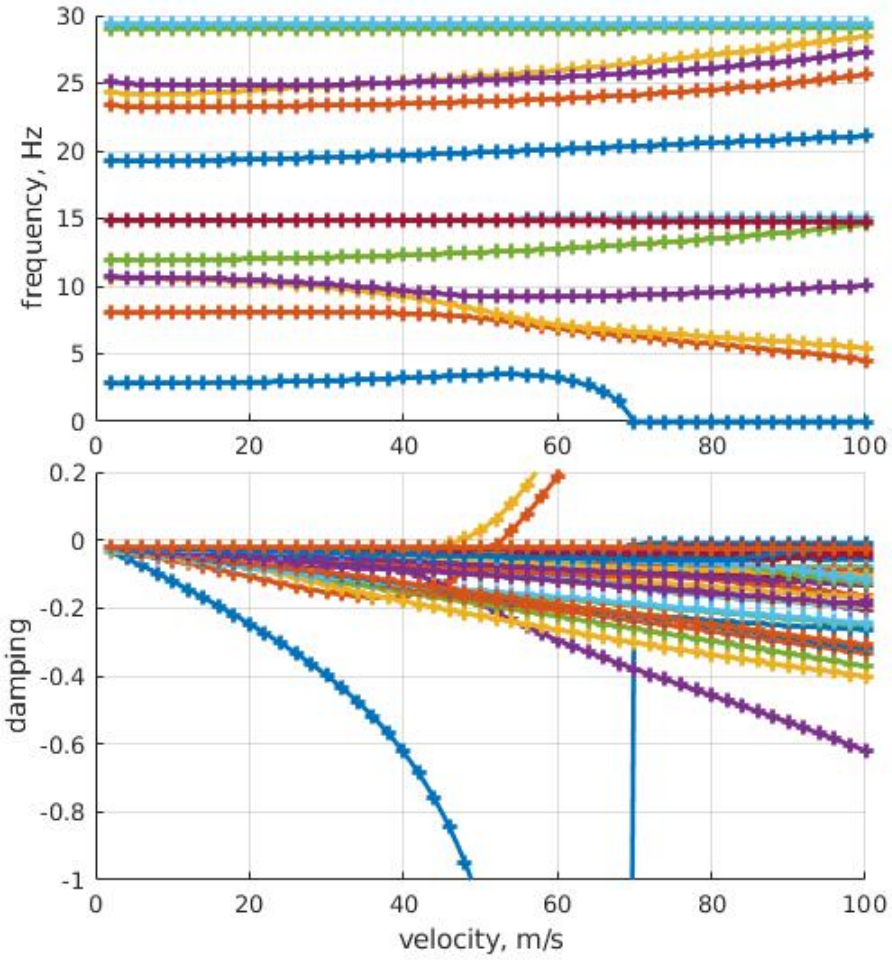

Figure 20: Aeroelastic frequency and damping vs airspeed for the nominal flutter configuration

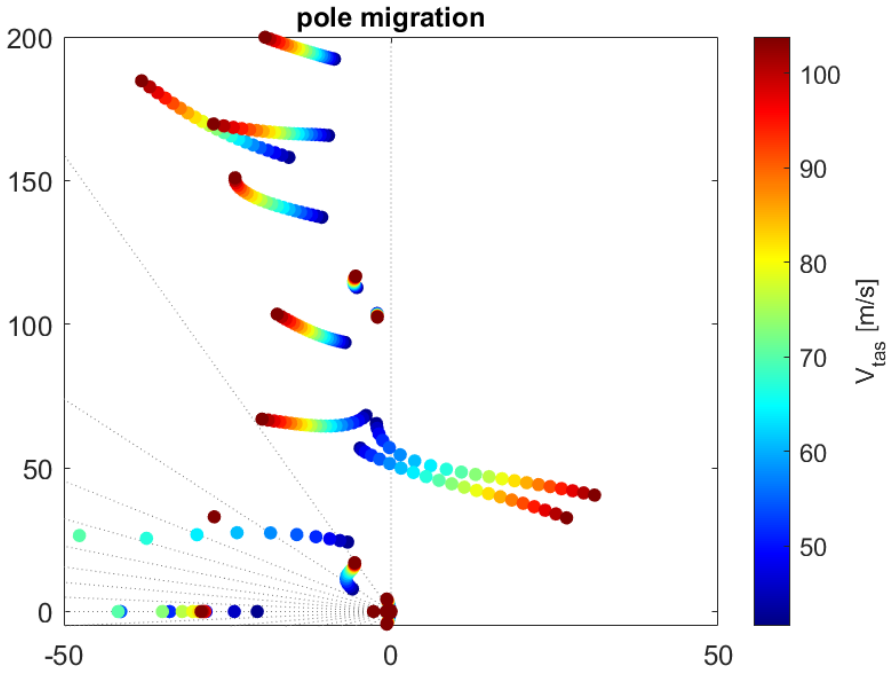

Figure 21: Pole migration for increasing airspeed

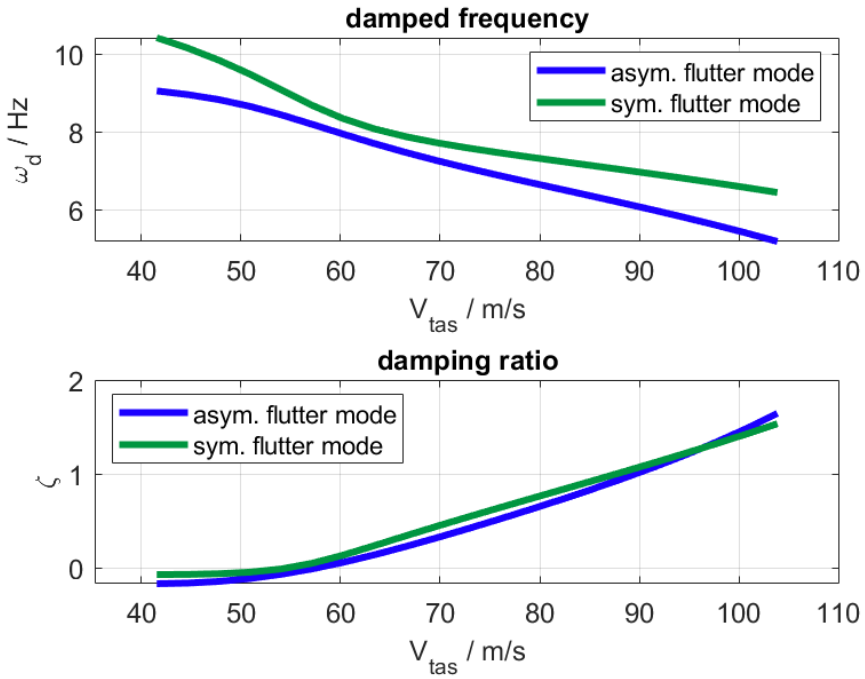

Figure 22: Change in damped frequency and damping ratio with respect to airspeed

5 Conclusion

This deliverable summarizes the steps of validation that have been performed in order to examine the maturity of the developed tools within the collaborative design process. Data generated from simulations, ground tests, or flight tests are used to achieve this goal. Furthermore, the models and methods are validated through comparisons between different techniques, tools, or simulations and test data.

The FE models are validated based on ground tests performed with the demonstrator aircraft, while for the aerodynamics different tools based on Computational Fluid Dynamics (CFD) and lifting line theory are compared with the collected flight test data. The methods used for structural and aerodynamic modeling have been found to be suitable for the collaborative design process. By leveraging the building blocks and expertise in flight dynamics, the ASE model of the aircraft is constructed using analytical models. These models have been updated and validated, e.g. by comparing the results of different flutter analysis methods.

The design of the flight control laws for the demonstrator also utilizes model-based tools, with their validation achieved through HIL and flight test campaigns. This confirms the reliability of the underlying ASE models and the design tools. Consequently, it can be concluded that parametric variations within the integrated design toolchain will yield well-performing closed-loop systems, making the results applicable for conceptual aircraft design.

6 Bibliography

[1] FEMTools Home Page.

[2] Brigitte Boden, Jan Flink, Robert Mischke, Kathrin Schaffert, Alexander Weinert, Annika Wohlan, Caslav Ilic, Tobias Wunderlich, Carsten M. Liersch, Stefan Görtz, Erwin Moerland, and Pier Davide Ciampa. Distributed Multidisciplinary Optimization and Collaborative Process Development Using RCE. In *AIAA Aviation 2019 Forum, 17–21 June 2019, Dallas, TX, USA*. American Institute of Aeronautics and Astronautics, 2019.

[3] Thomas Klimmek. Parameterization of Topology and Geometry for the Multidisciplinary Optimization of Wing Structures. page 9, 2009.

[4] Yasser M. Meddaikar, Johannes Dillinger, Thomas Klimmek, Wolf Krueger, Matthias Wuestenhagen, Thiemo M. Kier, Andreas Hermanutz, Mirko Hornung, Vladyslav Rozov, Christian Breitsamter, James Alderman, Bela Takarics, and Balint Vanek. Aircraft aeroservoelastic modelling of the FLEXOP unmanned flying demonstrator. In *AIAA Scitech 2019 Forum*. AIAA, jan 2019.

[5] Jurij Sodja, Roeland De Breuker, Yasser M. Meddaikar, Johannes K. Dillinger, Keith Soal, Yves Govers, Wolf Krueger, Panagiotis Georgopoulos, Christos Koimtzoglou, Christian Roessler, Sebastian J. Koeberle, Julius Bartasevicius, Daniel Teubl, Laszlo Gyulai, Szabolcs Toth, Mihaly Nagy, Daniel Balogh, Miklos Jasdi, Péter Bauer, and Balint Vanek. *Ground Testing of the FLEXOP Demonstrator Aircraft*.